Possible model of an antiferroelectric twist grain boundary phase

J. G. Meier,[1] M. Nobili,[2,*] T. Carlsson,[1] P. Rudquist,[1] A. S. Petrenko,[3] J. W. Goodby,[3] M. Brunet,[2] and S. T. Lagerwall[1]
[1]*Department of Microelectronics and Nanoscience, Chalmers University of Technology, S-41296 Göteborg, Sweden*
[2]*Laboratoire des Colloïdes, Verres et Nanomatériaux, Université Montpellier II/CNRS, 34090 Montpellier, France*
[3]*Department of Chemistry, University of Hull, Hull HU6 7RX, United Kingdom*
(Received 4 October 2006; published 13 July 2007)

Using x-ray and optical methods we have probed the structural organization of an antiferroelectric twist grain boundary phase (TGBC_a) lying between the regular antiferroelectric smectic-C (SmC_a^*) and the smectic-Q (SmQ) or isotropic phase. We find that the twist axis is everywhere perpendicular to the local smectic layer normal and that the helical superstructure is incommensurate with the smectic layer structure. The twist grain boundaries consist of a periodic lattice of alternating $+1/2$ and $-1/2$ dispirations, i.e., unit screw dislocations in combination with half unit disclinations. The molecular tilt plane is alternatingly parallel and perpendicular to the twist axis. We find that the optically measured tilt angle in the SmC_a^* phase is smaller than that measured by x rays, which is the opposite to what is found in the SmC^* phase. This means that the core part tilts less than the end chains in the SmC_a^* phase, while it tilts more in the SmC^* phase. On entering the TGB phase a clear decrease is measured in the tilt angle. This is explained by the elastic influence from the disclinations, which appear in this phase.

DOI: 10.1103/PhysRevE.76.011704 PACS number(s): 61.30.Eb, 61.10.Eq, 61.30.Cz, 61.30.Mp

I. INTRODUCTION

In 1988 Renn and Lubensky [1] published the first structural model corresponding to a liquid-crystalline phase analogous to the Abrikosov flux lattice phase, found in type-II superconductors, predicting it to exist between the smectic-A^* (SmA^*) and chiral nematic phases. The phase would consist of smectic blocks with the layer normal of the individual slabs being perpendicular to an axis around which they twist in a helical fashion (Fig. 1). Regularly spaced grain boundaries of parallel screw dislocations mediate the twist between the smectic blocks. Accordingly, the phase was named twist grain boundary (TGB) phase and, because it involves an orthogonal smectic, it is specified as the TGBA phase. The spacing period of screw dislocation sheets can be either commensurate or incommensurate with respect to the pitch of the helical superstructure of the phase.

The basic structural quantities of the TGB phase are (1) the smectic layer thickness—d, (2) the pitch of the helical superstructure—p, (3) the distance between two grain boundaries, equivalent to the thickness of a smectic block (the "coherence length" of the undisturbed smectic layers in the block)—l_b, (4) the distance between dislocation lines within the grain boundaries—l_d, (5) the twist angle between the layer normals of two consecutive smectic blocks—α (Fig. 1). These quantities are geometrically related by

$$\alpha = 2\arcsin\left(\frac{d}{2l_d}\right) \approx \left(\frac{d}{l_d}\right), \quad \alpha = \frac{2\pi l_b}{p}, \quad p = \frac{2\pi l_b l_d}{d}. \tag{1}$$

Further development of the theory led in 1992 to the prediction of two more TGB phases in the vicinity of the N^*-SmA^*-SmC^* triple point. The model comprises all features of the TGBA phase but the smectic blocks possess smectic-C (SmC) order. Hence, the molecular director makes an angle with the layer normal. Two distinctions can be made for this type of TGB phase with (a) the expulsion of the smectic-C^* helix in the blocks (TGBC phase) or (b) the incorporation of the smectic-C^* helix in the blocks (TGB$\tilde{C}$ phase) [2].

Goodby *et al.* [3,4] synthesized the first TGB material and reported the discovery of the TGBA phase existing between the SmA^* and the isotropic phase in 1989 shortly after the publication of the theoretical work by Renn and Lubensky [1]. The TGBC phase was discovered by Nguyen *et al.* [5] in 1992. Several authors reported, in addition to the already known textures of the TGBA and TGBC phases, a TGB phase with an apparent regular square or hexagonal grid pattern obtained in glass cells with planar anchoring conditions [6–8]. It has been discussed if those textures indicated a possible TGB$\tilde{C}$ phase.

High-resolution x-ray studies on oriented samples of the TGBA phase, performed by Srajer *et al.* [9], confirmed all the essential features of an incommensurate TGBA phase. The measured physical properties were very well described by the Renn-Lubensky model. On TGBC phases, detailed x-ray diffraction studies surprisingly revealed that these phases show commensurability [10,11]. Furthermore, in contrast to the original model by Renn [2], the TGBC phase was found to have the layer normal of the individual smectic-C blocks inclined with respect to the helix axis. The inclination angle of the layer normal is about the same as the tilt-angle of the molecules within the corresponding SmC^* phase. Additionally, the local $\vec{P}_s$ vector is perpendicular to the helix axis and rotates in a helical fashion around that axis. Hence, the tilt plane, spanned by the local director and the smectic layer normal, is essentially perpendicular to the grain boundaries [12,13]. It has been discussed if polar interactions are the origin of the commensurate lock-in mechanism. However, the origin of commensurability in TGB phases is still

*Corresponding author. nobili@lcvn.univ-montp2.fr

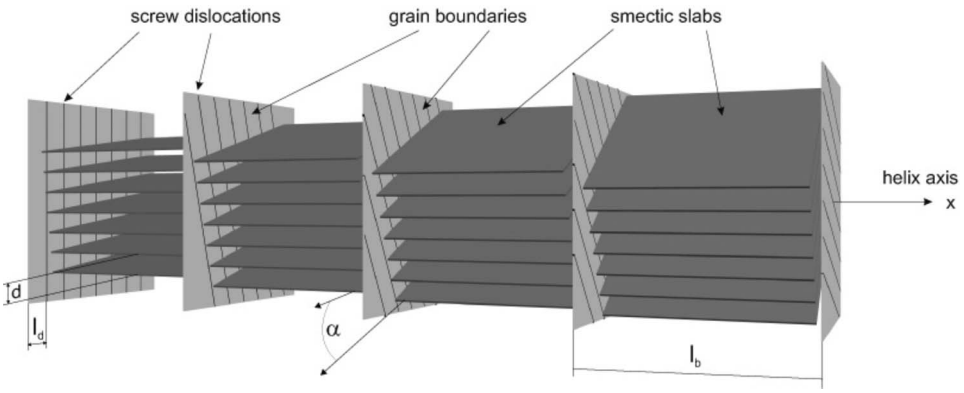

FIG. 1. Generic model of TGB phases according to Renn and Lubensky.

unclear, since in later studies, a commensurate TGB*A* phase was observed as well [14].

In addition to the theoretically predicted TGB*A*, TGB*C*, and TGB$\tilde{C}$ phases, recently a new type of a twist grain boundary phase with a local antiferroelectric structure (TGBC_a) has been discovered [15,16] in the compound depicted in Fig. 2. This phase lies between the regular antiferroelectric SmC_a^* and the Sm*Q* phase. The Sm*Q* phase has been identified as a smectic blue phase with antiferroelectric order [17,18].

By studying the optical textures and the electric-field induced effects in this phase we developed a qualitative model of the microscopic organization of the TGBC_a phase [19]. The layer normal of the individual smectic blocks is perpendicular to the helix axis. Inside the smectic blocks the molecular tilt plane of the local anticlinic structure is parallel to the grain boundary of the TGBC_a phase. The grain boundaries consist of a regular lattice of +1/2 and −1/2 dispirations; i.e., unit screw dislocations combined with half unit disclinations. Whereas all screw dislocations have the same sign, the sign of the half unit disclinations alternates in adjacent dispirations. Hence, in the grain boundaries the molecular tilt plane between adjacent dispirations is alternately parallel and perpendicular to the TGB helix, cf. Fig. 3. In this figure l_1 and l_2, which cannot *a priori* be considered equal, correspond to l_d in Fig. 1.

In this paper we report quantitative results of small-angle x-ray scattering (SAXS) and optical experiments performed on powder and oriented samples of the TGBC_a phase.

II. EXPERIMENTAL

A. Optical measurements

1. Pitch measurement

The selective reflection wavelengths were measured using a Shimadzu UV-3100 UV/VIS/NIR spectrophotometer fitted with a Mettler FP52 hot stage and controller unit Mettler FP5. The temperature was independently measured using a PT100 temperature sensor providing a reproducibility and stability accuracy of 0.05 K for the hotstage subset. The liquid crystal has been studied in a commercial (E.H.C.) cell of thickness 4 μm. The results are represented in Fig. 4.

2. Optical tilt-angle measurement

A computer-controlled setup was assembled consisting of a HeNe laser with a $\lambda/4$ plate, giving circularly polarized light, two nicols mounted on computer-driven rotators with an angular resolution better than 0.01°, a Mettler hotstage and controller as described above, and a photodetector connected to the computer via a two-channel memory oscilloscope.

A cell with transparent ITO electrodes and a cell gap of approximately 1 μm was prepared. The inner cell surfaces were coated with polyimide, which was antiparallel buffed to give planar anchoring conditions and a surface-stabilized state with preferred director orientation. The cell was introduced into the hotstage subset, which was mounted between the crossed nicols and aligned in the optical path for normal incident light. Thus, the liquid-crystal cell acts as a switchable birefringent slap.

The sample was switched with a square ac field (E =12.5 V/μm; f=110 Hz), generated with a leader function generator LFG 1300 and voltage amplifier F20ADI from FLC Electronics. The light-intensity modulation and the electric field was recorded by the two-channel memory oscilloscope. The computer drives the polarizers and registers the light intensity and rotator settings. The program separates the optical signal according to the two switching states for the angular settings of the polarizers. The polarizers were rotated over 90° in steps of 10° giving ten independent data points for each temperature. The plots of each switching state versus the polarizer position were fitted to $\sin^2$ functions and the phase shift between the functions for the two switching states were determined. The phase shift is equal to twice the tilt angle [20]. The method provides an accuracy and reproducibility of the tilt angle better than 0.5°.

B. Small-angle x-ray scattering (SAXS)

X-ray experiments were performed using a Cu K_α radiation of an 18 kW rotating anode x-ray generator (Rigaku RU-200). We use a source with apparent dimensions 0.3

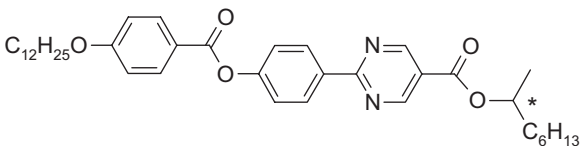

FIG. 2. Molecular structure of the studied compound. The phases and transition temperatures are isotropic, 93.1 °C Sm*Q*; 92.9 °C, TGBC_a; 91.6 °C, SmC_a^*; 68.3 °C, crystalline, melting point 86.4 °C.

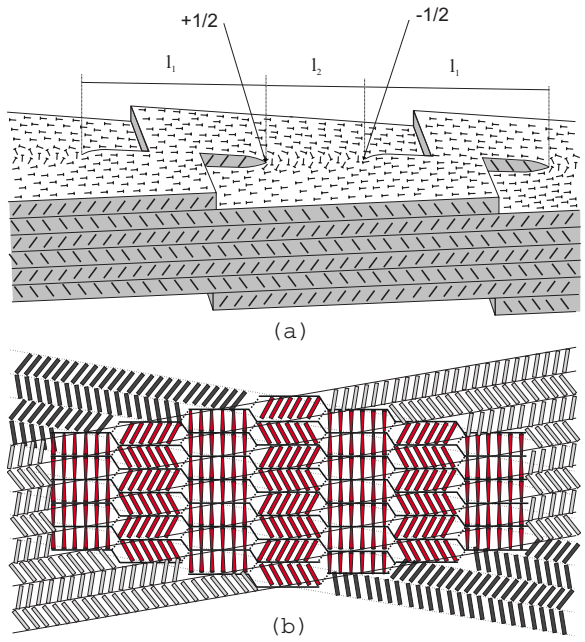

FIG. 3. (Color online) (a) Model of the TGBC_a phase in which the layers are cut parallel to a grain boundary. The lengths l_1 and l_2 correspond to l_d in Fig. 1, while l_b would run perpendicular to the cut (the depth dimension). (b) Proposed director field (red) inside the grain boundary between two smectic blocks (black and gray).

$\times 0.3$ mm^2 operating at a working power of 3.2 kW. An osmic confocal max-flux optics was used as monochromator ($\Delta k_{\mathrm{FWHM}}=2\times10^{-2}$ Å^{-1}) and to focus the x-ray beam on a Schneider image plate. The sample was mounted on a phi goniometer coupled with a stepping motor providing 0.01° angular steps. The beam size at the sample position has a diameter of 0.8 mm.

1. Smectic layer spacing

The material was inserted in a Lindemann capillary of diameter 1 mm and wall thickness 0.01 mm. The sample was inserted into a Mettler FP52 hot stage with temperature control unit Mettler FP5. The windows of the hot stage were covered with metallized Kapton foil to prevent temperature gradients due to convection. The sample was then heated into the liquid state and allowed to crystallize again, creating a compact, polycrystalline sample. The scattering intensities were recorded with the image plate in the liquid-crystalline state for various temperatures.

2. ω scan

A cell was prepared from two cover glasses. The thickness of the glass was about 150 μm. A window of approximately 50 μm wall thickness was etched into each glass. To impose planar anchoring conditions (with smectic layer normal along the bounding surface), the inner surface of the cell was coated with polyvinyl alcohol (PVA) and thereafter buffed. The gap of the cell was approximately 25 μm, maintained by spacer balls mixed into the glue used to assemble the cell. The glass sheets were assembled such that the buffing direction of the PVA layers were parallel to each other. The cell was then filled by capillary force with the liquid crystal being in the isotropic liquid state. Very good alignment was achieved by cooling down the material into the SmC_a^* phase followed by three slow heating (cooling) cycles over the SmC_a^*-TGBC_a phase transition. The quality of the alignment was checked under a microscope. In the TGBC_a phase the material then exhibited a texture with large Grandjean monodomains separated by oily streak defect lines. The sample was then inserted into a two stage oven allowing a temperature regulation within a 20 mK accuracy. Placement and alignment of the sample was checked by means of an endoscope camera granting that only one large Grandjean monodomain was irradiated by the x-ray beam.

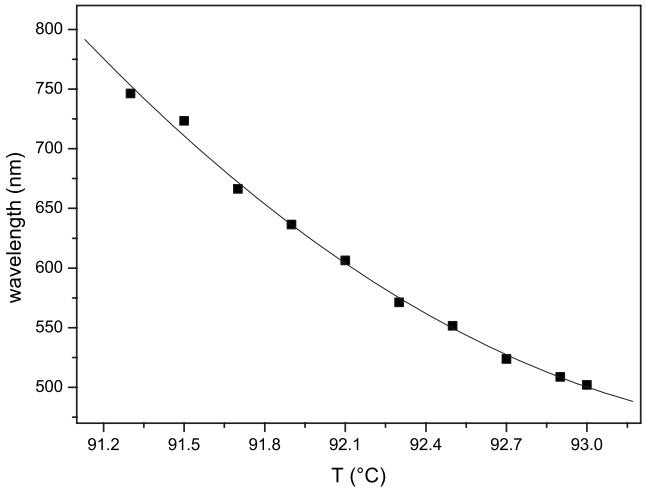

FIG. 4. Wavelengths of the selectively reflected light of the Grandjean planar texture of the TGBC_a phase as a function of temperature.

III. RESULTS AND DISCUSSION

To test our model of the TGBC_a phase, we measured the pitch of the helical superstructure p, the smectic layer thickness d, and the coherence length ξ (spatial extension) of the smectic blocks. These are the characteristic lengths of the phase, which are accessible by visible and x-ray radiation studies. Additionally, we measured the apparent optical tilt angle θ_{opt} of the synclinic states under an applied electric field, which gives a good estimate of the undisturbed molecular tilt in the SmC_a^* and TGBC_a phases.

A. Measurements of p, d, θ_{opt}

The pitch of the TGB helix was determined by measuring the wavelength of the selectively reflected light observed as a dip in the transmission spectrum at normal incidence in the Grandjean texture. In this geometry the spectrometer reading λ is related to the helical pitch p of the liquid-crystal phase according to $\lambda=\bar{n}p$. Assuming an average refractive index $\bar{n}$ of 1.5 the pitch of the helical superstructure varies from about 500 nm close to the phase transition to the SmC_a^* phase to 330 nm close to the isotropic liquid (Fig. 4).

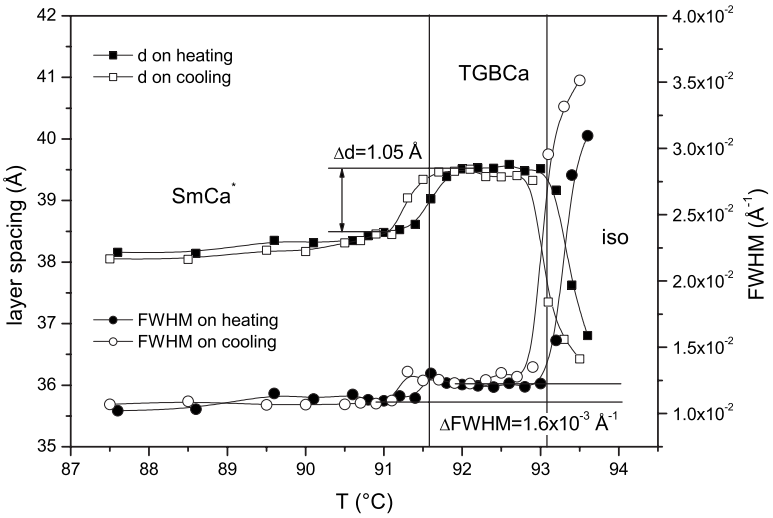

FIG. 5. Smectic layer spacing in dependence of the temperature. Gaussian functions have been fitted to the scattering profiles yielding the peak center, giving the d value, and the peak width (FWHM).

The evolution of the smectic layer spacing across the phase transitions was directly measured by small angle x-ray scattering of a nonoriented, polydomain sample. As depicted in Fig. 5, the d value of the smectic layer periodicity shows only a minute dependence on the temperature within the range of the SmC_a^* or the TGBC_a phase. Around the phase transition from SmC_a^* to TGBC_a a sudden change of the layer spacing of about 1 Å occurs. A slight hysteresis of 0.3 K is apparent between the heating and cooling curves. The phase transitions are also clearly marked by a distinct change of the full width at half maximum (FWHM) of the scattering profiles. Also the width of the profiles shows no dependence of the temperature in the SmC_a^* or the TGBC_a phase but it increases upon the transition from the SmC_a^* to the TGBC_a. This behavior is related to a decrease of smectic order in the TGBC_a phase due to the occurrence of grain boundaries. In the isotropic liquid the profile becomes broad due to the loss of positional correlation typical for a liquid phase.

When subjected to an external electric field above the threshold for the transition from the anticlinic to synclinic state, the material exhibits three-state optical switching in bookshelf geometry, giving two $\vec{P}_s$-current peaks per half period of the driving field over the entire range of the SmC_a^* and the TGBC_a phase [19]. Therefore, the molecular arrangement, also in the TGBC_a phase, must possess a molecular tilt, which is anticlinic in adjacent layers. The angular difference between the two synclinic states as probed by the direction of their dielectric tensors at optical wavelengths can be considered as twice the value of the tilt. We call the tilt angle deduced this way the optical tilt. On the other hand, the tilt angle can also be deduced comparing the x-ray measured layer spacing (d) of the tilted phase with the layer spacing in the SmA phase. Unfortunately our compound does not show a SmA phase. Nevertheless, an estimation of the layer tilt angle can be obtained by replacing the SmA layer thickness with the length of the molecule (l) as follows:

$$\theta = \arccos(d/l). \tag{2}$$

The molecular length has been determined by molecular modeling to be about 42 Å. The tilt angle, deduced from the x-ray experiment gives an average inclination of the entire molecule. This results in numerically different values for the tilt-angle obtained by either of the methods. A detailed treatment of this problem for the smectic-A^*-C^* transition is given by Gießelmann and Zugenmaier [21].

In Fig. 6 the optical tilt angle and the tilt angle deduced from the layer spacing are shown in the dependence of the temperature. The important feature in Fig. 6 is the optical tilt angle continuous decrease with increasing temperature over the entire range of the SmC_a^* and the TGBC_a phases. This is strong evidence that the symmetry of both phases is the same as a field-induced SmC_a^* phase replaces the TGBC_a. At the transition to the isotropic liquid the tilt angle goes to zero but the transition is shifted by about 0.5 K to higher temperatures under the influence of the external field [19]. The increase of $\theta_{x\ ray}$ in the isotropic liquid is an artifact due to a seemingly reduced d value when the smectic long-range order is replaced by short-range order (smectic fluctuations).

It is a well-known observation that x-ray tilt angles and optical tilt angles do not coincide. In the smectic-C^* phase it

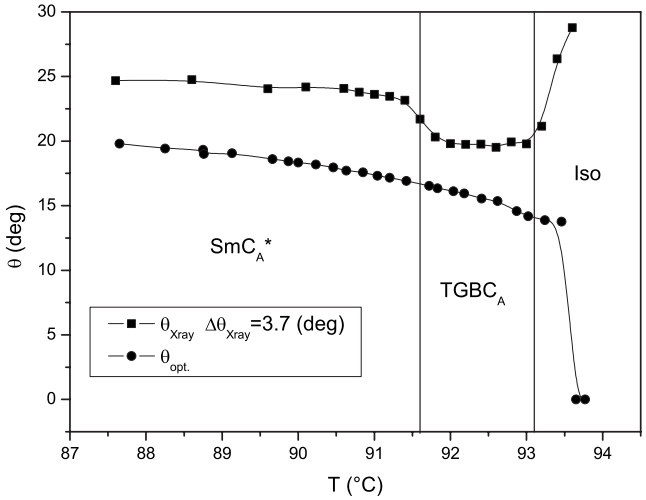

FIG. 6. The tilt angle in dependence of the temperature as deduced from the d values of the SAXS experiment ($\theta_{x\ ray}$) and from the electro-optic switching (θ_{opt}) of the synclinic states.

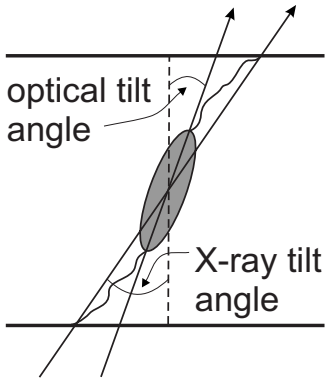

FIG. 7. The optical tilt angle is mainly determined by the dielectric tensor of the mesogenic core. The x-ray tilt angle is deduced from the center of mass distribution of the molecules, giving the layer spacing, and the molecular length.

is always found that $\theta_{x\ ray} < \theta_{opt}$. This is explained by the fact that the core part of the molecule, which gives the main contribution to the dielectric tensor, tilts more than the end chains of the molecule. The end chains are thus more perpendicular to the layers, which favors a phase sequence *N*-*A*-*C* or *N*-*C*, as both transitions $A \leftrightarrow N$ and $C \leftrightarrow N$ are permeation transitions.

In striking contrast, in this case we have $\theta_{x\ ray} > \theta_{opt}$ as seen from Fig. 6. This means that in the SmC_a^* phase the core of the molecule is *less* inclined than the end chains, as depicted in Fig. 7. With the admitted simplification in this figure, that both end chains tilt identically, it shows the general feature that $\theta_{x\ ray} > \theta_{opt}$. In reality, the nonchiral end chain seems to behave somewhat differently from the chiral one, which may tilt as much as nearly being orthogonal to the core [22]. Anyway, the fact that $\theta_{x\ ray} > \theta_{opt}$ in the whole temperature range of anticlinic order shows that this order is characterized by an average tilt of the end chains that is larger than that of the core. This is in agreement with the picture that no nematic phase appears in antiferroelectric liquid-crystal materials due to the molecular shape [23].

In Fig. 6 we also note a decrease, $\Delta\theta_{x\ ray}$, in the x-ray tilt angle at the transition between the SmC_a^* and the TGBC_a phase. Equation (2) thus implies a corresponding decrease Δd,

$$\Delta d = -l \sin \theta_t \Delta\theta_{x\ ray}, \tag{3}$$

in the smectic layer spacing, θ_t being the tilt close to the transition. Such a behavior is not observed in the tilt deduced from the electro-optic switching measurements. The reason for the decrease in $\Delta\theta_{x\ ray}$, and the absence of such an effect in $\Delta\theta_{opt}$ can be understood qualitatively beginning with the comment already given above: the optical measurements are performed by applying an external electric field, strong enough to guarantee that the *c* director is uniform within each smectic layer at all times. Thus, in this case there is no TGB structure in the temperature interval 91.6 °C–93.1 °C, but just untwisted SMC_a^*. The x-ray measurements, on the other hand, are performed without any applied external electric field. In this case the *c* director can be expected to be uniform within each smectic layer in the SmC_a^* phase, while in the TGBC_a phase, on the other hand, the *c* director is nonuniform, performing a 180° rotation around each dispiration line as is depicted in Fig. 3. Such a rotation increases the elastic energy of the system. Generally speaking, a deformation in the *c*-director field costs more energy the higher the value of the tilt angle. The corresponding elastic constants B_i can be shown [24,25] to exhibit a tilt dependence according to $B_i = \bar{B}_i \theta^2$, where $\bar{B}_i$ can be assumed to be tilt independent. Thus, decreasing the tilt reduces the elastic energy of the system. On the other hand, changing the tilt from its equilibrium value increases the corresponding Landau energy of the system [26]. Minimizing the sum of the elastic contribution to the energy and the Landau energy, the system will find a new equilibrium tilt angle, thus adopting a value of θ, which is smaller by the amount of $\Delta\theta$ than what otherwise would have been expected. From Fig. 3 we note that near the grain boundary the smectic layers in each region of length l_1 will be under compression, while in each region of length l_2 they will be under dilatation. Therefore, θ will be, respectively, larger and smaller in these regions, as compared to the equilibrium angle. This might somewhat broaden the θ distribution but will have little influence on the shift $\Delta\theta$. To estimate this shift we thus only need a single model, which takes the *c*-director field into account.

B. TGB influence on the tilt angle

In order to make an estimation of $\Delta\theta_{x\ ray}$ we perform a calculation using a simplified model of the system. In this model a one-layer thick, circular slab of SmC_a^* (it is then equivalent to SmC^*) is studied. The radius of the slab is denoted *R* and corresponds to the distance l_d between dislocation lines within the grain boundaries as defined by Fig. 1. Studying small deviations $\delta\theta = \theta - \theta_0$ of the tilt from its equilibrium value, the free-energy density g_L is expanded around θ_0 as

$$g_L(\theta) = g_0 + a_0(\theta - \theta_0)^2. \tag{4}$$

In the case of the Sm*C* phase, the coefficient a_0 would be the same as the one appearing in the first term, $1/2 a_0 \theta^2$, of the Landau expansion around the Sm*A*-Sm*C* transition.

In Fig. 3 we see that the *c* director in the TGBC_a phase, by topological reasons, is forced to make a π rotation around the dispiration lines. Below is shown, that this distortion of the *c* director influences the system in such a way that the tilt decreases slightly from its equilibrium value θ_0. In order to estimate this change in tilt, a simple model calculation is performed below.

The system studied in this calculation is defined by Figs. 8 and 9. In our domain consisting of a one-layer-thick, circular slab of radius *R*, the screw dislocation line goes through the center of the domain. The normal to the smectic layers is described by a unit vector $\boldsymbol{a}$. Neglecting the fact that, due to the screw dislocation, $\boldsymbol{a}$ is a slowly varying function when going around the dislocation line, we consider a flat layer according to Fig. 9. A Cartesian coordinate system is introduced in such a way that the smectic slab is parallel to the (x,y) plane and the layer normal falls along the positive

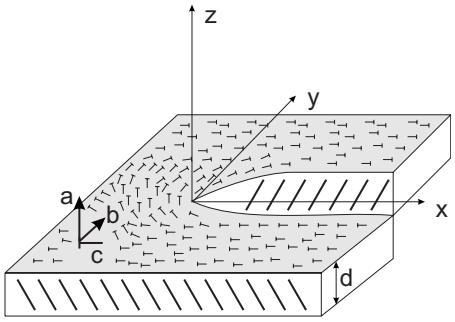

FIG. 8. The dispiration is contained in a volume defined by l_b, l_d, and d. It has been found that in the case of TGB*A* phases $l_b \approx l_d$ [14].

z axis, i.e., $\boldsymbol{a}=\hat{\boldsymbol{z}}$. For mathematical convenience a third unit vector $\boldsymbol{b}$ is also introduced according to

$$\boldsymbol{b}=\boldsymbol{a}\times\boldsymbol{c}, \tag{5}$$

$\boldsymbol{c}$ being the c director. The three vectors $\boldsymbol{a}$, $\boldsymbol{b}$, and $\boldsymbol{c}$ are then given by

$$a_x=0, \quad a_y=0, \quad a_z=1,$$

$$b_x=-\sin\frac{1}{2}\phi(z), \quad b_y=\cos\frac{1}{2}\phi(z), \quad b_z=0,$$

$$c_x=\cos\frac{1}{2}\phi(z), \quad c_y=\sin\frac{1}{2}\phi(z), \quad c_z=0. \tag{6}$$

Due to the symmetry of the system studied, the calculation of the elastic distortion energy is most easily performed by using the cylindrical polar coordinate system depicted in Fig. 9, in which the three vectors $\boldsymbol{a}$, $\boldsymbol{b}$, and $\boldsymbol{c}$ can be expressed as

$$a_r=0, \quad a_\phi=0, \quad a_z=1,$$

$$b_r=\sin\frac{1}{2}\phi(z), \quad b_\phi=\cos\frac{1}{2}\phi(z), \quad b_z=0,$$

$$c_r=\cos\frac{1}{2}\phi(z), \quad c_\phi=-\sin\frac{1}{2}\phi(z), \quad c_z=0. \tag{7}$$

The elastic energy per unit volume is now given by

$$g^{el}=\frac{1}{2}B_1(\boldsymbol{\nabla}\cdot\boldsymbol{b})^2+\frac{1}{2}B_2(\boldsymbol{\nabla}\cdot\boldsymbol{c})^2, \tag{8}$$

where B_1 and B_2 are the elastic constants for the bend and splay of the c director within a smectic layer, respectively [27]. Substituting the ansatz (7) into Eq. (8) we derive the elastic energy density of the system as

$$g^{el}=\frac{1}{8r^2}\left[B_1\sin^2\frac{1}{2}\phi(z)+B_2\cos^2\frac{1}{2}\phi(z)\right]. \tag{9}$$

With the one constant approximation $B_1=B_2=B$, which scales as $B=\bar{B}\theta^2$, we then obtain

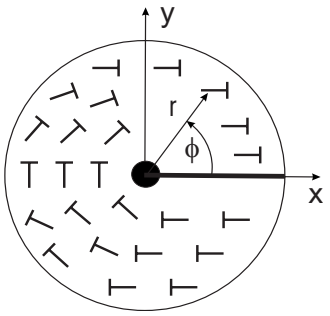

FIG. 9. The c director rotates by 180° when going around the center of the slab. The size R of the domain is of the order of the distance l_d between dislocation lines within the grain boundary. For simplicity we consider a symmetric volume $V=\pi R^2 d$.

$$g^{el}=\frac{\bar{B}}{8r^2}\theta^2. \tag{10}$$

As is seen from Eq. (10) the elastic energy per unit volume is r dependent. The average value of the quantity, which we denote by g^{el}_{av}, is now calculated as

$$g^{el}_{av}=\frac{G^{el}}{V}, \tag{11}$$

where $V=\pi R^2 d$ is the volume of the domain and G^{el} is the total elastic energy stored in the domain,

$$G^{el}=\int_V g^{el}dV. \tag{12}$$

When evaluating the integral (12) we must exclude a cylinder with a radius r_0 of some molecular dimensions around the dispiration core where the c director is singular. The total elastic energy of one domain is now given by

$$G^{el}=\int_{r_0}^{R}\int_0^{2\pi}\int_0^d g^{el}r dr d\phi dz=\frac{1}{4}\bar{B}\theta^2\, d\pi\ln\frac{R}{r_0}, \tag{13}$$

and the average elastic energy density becomes

$$g^{el}_{av}=\frac{G^{el}}{\pi R^2 d}=\frac{\bar{B}}{4R^2}\ln\frac{R}{r_0}\theta^2. \tag{14}$$

By taking the block size l_b equal to the dispiration distance l_d as in the TGB*A* phase we can estimate R and r_0 to be $R \approx 200$ Å and $r_0 \approx 30$ Å implying $\ln\frac{R}{r_0}\approx 2$ and the average elastic energy density is

$$g^{el}_{av}=\frac{\bar{B}}{2R^2}\theta^2. \tag{15}$$

The expression of the average tilt of the system exhibiting the distorted c director according to Fig. 9 is calculated by minimizing the total energy density

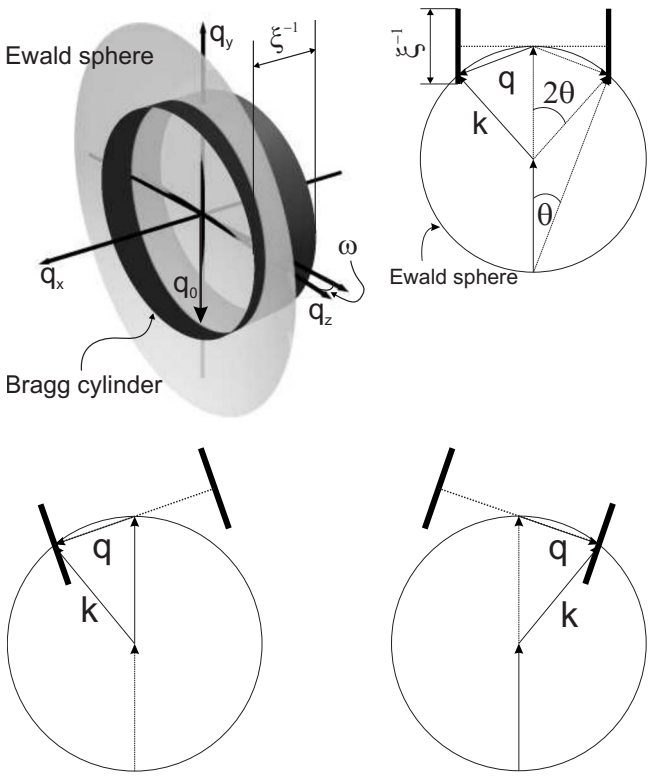

FIG. 10. Scattering geometry.

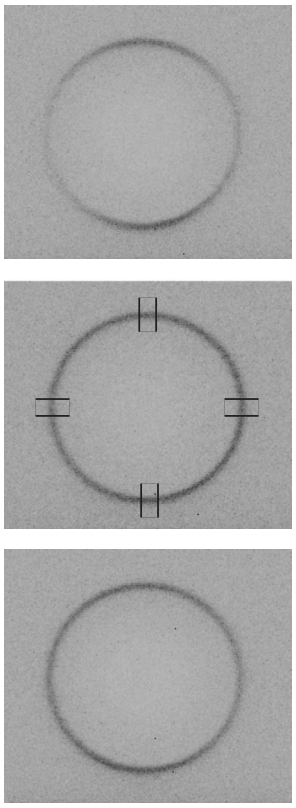

FIG. 11. Example of an ω scan; $(T-T_c=0.8\ \mathrm{K})$.

$$g(\theta) = g_L(\theta) + g_{av}^{el}(\theta) = g_0 + a_0(\theta - \theta_0)^2 + \frac{\bar{B}}{2R^2}\theta^2, \quad (16)$$

with respect to θ. In this way the average tilt θ_{TGB} is calculated as

$$\theta_{TGB} = \frac{a_0}{a_0 + \dfrac{\bar{B}}{2R^2}}\theta_0. \quad (17)$$

Thus, the θ^2 dependence of the elastic constant forces the average equilibrium tilt of the system to be shifted toward a smaller value according to

$$\theta_{TGB} = \theta_0 - \delta\theta. \quad (18)$$

As $\delta\theta/\theta_0$ is expected to be a small quantity we expand Eq. (18) in the limit $\frac{\bar{B}}{2R^2} \ll a_0$ and calculate the following expression for the relative shift of the equilibrium tilt as

$$\frac{\delta\theta}{\theta_0} \approx \frac{\bar{B}}{2a_0R^2}. \quad (19)$$

C. Measurement of ξ

The x-ray structure factor of a TGB phase qualitatively depends on the value of the ratio $\alpha=\Delta\theta/2\pi$. If α is irrational the TGB lattice is incommensurate, if α is rational, i.e., $\alpha=p/q$ with p and q mutually prime integers, the lattice is commensurate with a q-fold screw axis.

In the case of a commensurate TGB structure, the fundamental set of reciprocal vectors forms a ring of equispaced Bragg spots in the plane (q_y,q_z) perpendicular to the pitch direction, provided that the individual smectic blocks have their layer normal perpendicular to the helix axis. If the TGB lattice is incommensurate, scattering is intense on a Bragg cylinder of axis x and radius $q_0=2\pi/d$ as sketched in Fig. 10. In the TGBA phase the cylinder has a Gaussian profile along q_x of characteristic width

$$\xi^{-1} = 2\pi/\sqrt{(pd)}, \quad (20)$$

where p is the pitch just below the transition from the TGBA to the cholesteric phase in the Renn-Lubensky model [1]. If l_b is assumed to be equal to l_d in Eq. (1) then the relation between the coherence length ξ and the thickness l_b of a smectic block is given by $l=\sqrt{2\pi/\xi^{-1}}$.

This profile has been determined by measuring the scattering intensity at constant momentum transfer in dependence of the rocking angle ω in well-aligned samples for three different temperatures: (i) just above the transition $\mathrm{Sm}C_a^* \rightarrow \mathrm{TGB}C_a$ $(T-T_c=0.2\ \mathrm{K})$, (ii) the middle of the temperature range of the TGBC_a phase $(T-T_c=0.8\ \mathrm{K})$, and (iii) close to the transition to the isotropic liquid $(T-T_c=1.4\ \mathrm{K})$.

Figure 11 shows records of the scattering intensity for $\omega=0°$ and $\omega\pm10°$ at $T-T_c=0.8$ K. For $\omega=0$ a ring is obtained with a constant scattering intensity around its circumference. No evidence for a commensurate structure could be found.

For rocking angles different from zero the intensity decreases at the horizontal areas (along q_z) while it remains constant at the vertical areas (along q_y), cf. Fig. 10. To quantify the scattering intensity, we measured the intensity on

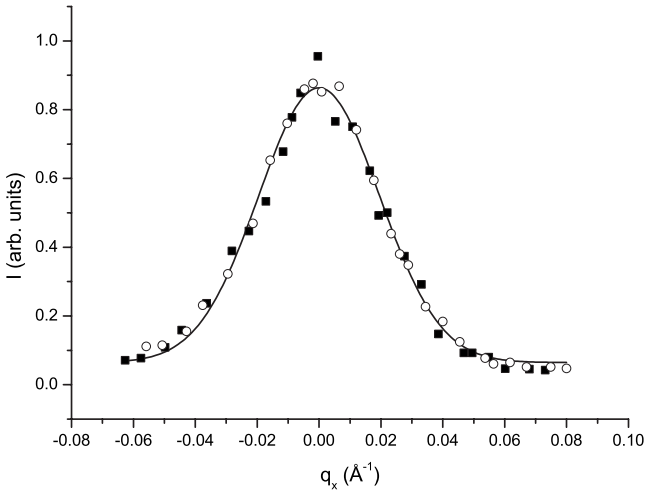

FIG. 12. Intensity in dependence of the rocking angle ω in units of q_0 and Gaussian fit to the data. The two sets of data points are obtained from the left side (■) and the right side (○) of the ring. The fit of Eq. (22) to the data points yields $q_c=0$ Å^{-1}; $\sigma=0.028$ Å^{-1}.

four areas along the scattering ring in Fig. 11: the left (L) and right (R) regions along q_z and the top (T) and bottom (B) ones along q_y. For each angle ω we calculated the normalized intensity $I^N_{L/R}(\omega)$ according to the equation

$$I^N_{L/R}(\omega) = \frac{I_{L/R}}{(I_T/2 + I_B/2)}, \tag{21}$$

where I_T and I_B are, respectively, the scattering intensities on the top and bottom regions of the ring.

This gives two identical ω curves, one for the left and right area, respectively. All ω scans yielded intensity distributions with a typical bell shape, centered around q_c with q_c being close to zero. Fitting the data points to a Gaussian function of the form

$$f(q_x) = y_0 + Ae^{[-(q_x - q_c)^2]/\sigma^2} \tag{22}$$

gives a numerical value for the center $q_c=0$ Å^{-1} and the characteristic width $\sigma=0.028$ Å^{-1} of the profile (Fig. 12). No significant temperature dependence of the characteristic width for the different ω-scan curves has been detected.

Summarizing we can state that the scattering pattern we obtained is that of an incommensurate TGB phase. The ω scan revealed that the twist axis of the helical superstructure is perpendicular to the layer normals of the individual smectic blocks like in the TGBA phase. The width of the Bragg cylinder remains constant over the temperature range of the TGBC_a phase. In conclusion, the structural results obtained by x ray are compatible with an anticlinic TGB phase (TGBC_a) as revealed by the electro-optic measurements [19].

IV. CONCLUSIONS

The model of the antiferroelectric TGB phase is very similar to the Renn-Lubensky model of the TGBA phase. The main differences are that the smectic blocks consist of SmC^*_a units and therefore, the grain boundaries are constituted by a regular lattice of $+1/2$ and $-1/2$ dispirations. Since resonant x-ray scattering is the only way to probe the anticlinic structure of the smectic slabs directly, we rely on measurable effects due to the structure of the grain boundaries or the smectic blocks.

The measured value of ξ^{-1} obtained from the ω scans is 0.028 Å^{-1}. This corresponds to an l_b value of about 90 Å, which appears rather low. The ω curve is the convolution of the true intrinsic width σ_{int} of the scattering profile along q_x and the experimental resolution $\sigma_{res}=0.01$ Å^{-1}. A reasonable estimation of the intrinsic width is $\sigma_{int}=\sigma-\sigma_{res}=0.018$ Å^{-1}, which gives $l_b=140$ Å close to typical values in TGBA phases (185 Å) [4,8,9].

In Sec. III B, we attributed the sudden increase of the layer spacing and therefore, the decrease of $\theta_{x\ ray}$, at the SmC^*_a to TGBC_a phase transition, to the occurrence of dispirations introducing a distortion in the c-director field (cf. Fig. 3). In order to estimate $\delta\theta$ from Eq. (19) we choose $\theta_0=23°$ from Fig. 6 and estimate R to about 160 Å. The material parameter values are estimated from data for DOBAMC (p-(n-decyloxybenzylidene - p - amino - (2 - methylbutyl) -cinnamate) found by different authors, assuming that these data, valid for one case of SmA^*-SmC^* transition, would indicate the order of magnitude also in this case. With $\bar{B} \approx 10^{-11}$ N [28], and $a_0 \approx 10^5$ N/m^2, which corresponds to the equilibrium tilt value 23° for DOBAMBC at 6 K below the tilting transition [26,29,30], we find $\delta\theta$ to be about 4.5°. This more than reasonable agreement with the experimentally found 3.7° is certainly fortuitous, considering the uncertainty in the parameter values, but supports our model of dispirations forming the grain boundaries.

Let us now look at the TGBC phase. It exhibits a much larger coherence length of the smectic blocks than the TGBA phase although the phase possesses a molecular tilt. It also has been shown that the normal of the molecular tilt plane is perpendicular to the TGB helix but the smectic layer normal of the individual blocks is inclined by about the molecular tilt with respect to the TGB helix. As a result, $\boldsymbol{n}$ is always perpendicular to the helix axis and the local polarization vector of the blocks, $\vec{P}_s$, spirals around the helix axis canceling any macroscopic polarization. It has been argued that the bend term in the elastic energy is lower in the situation where $\boldsymbol{n}$ is perpendicular and thus the tilt plane is parallel to the twist axis [12,31].

It is interesting to note that the TGBC phase prefers a situation in which the tilt plane is parallel to the helix axis even though an arrangement with the tilt plane being perpendicular to the TGB axis would be topologically possible as well (the original Renn-Lubensky model). The c director plays no role in the configuration of the grain boundary and it is therefore very similar to the TGBA phase. Thus, one is tempted to say that the following requirements must be met for a TGB phase: (1) $\boldsymbol{n}$ must be perpendicular to the TGB helix axis and (2) the macroscopic polarization must be zero.

If we apply these rules to the TGBC_a phase we shall have blocks with an anticlinic order and hence, zero polarization. The tilt plane and hence, $\boldsymbol{n}$ shall be perpendicular to the TGB axis. This is no problem within the smectic blocks.

At the grain boundary all these requirements can only be met when the tilt plane is parallel to the helix axis exclusively. This would require dislocations with a Burgers vector b equal to two. However, the elastic energy is quadratic in the Burgers vector; furthermore we estimated the smectic block size to four layers, which means that the smectic block would be just twice as thick as the grain boundary it self. Therefore, an arrangement with $b=1$, where half of the dislocations still produce a tilt plane in the low-energy orientation seems favorable.

ACKNOWLEDGMENTS

Financial support from the EU TMR program ORCHIS, the Swedish Foundation for Strategic Research, and the University of Hull Overseas Research Student Scheme is gratefully acknowledged. We are also very indebted to Frank Gießelmann, who greatly contributed to the automation and programming of the tilt-angle setup.

[1] S. R. Renn and T. C. Lubensky, Phys. Rev. A **38**, 2132 (1988).
[2] S. R. Renn, Phys. Rev. A **45**, 953 (1992).
[3] J. W. Goodby, M. A. Waugh, S. M. Stein, E. Chin, R. Pindak, and J. S. Patel, J. Am. Chem. Soc. **111**, 8119 (1989).
[4] J. W. Goodby, M. A. Waugh, S. M. Stein, E. Chin, R. Pindak, and J. S. Patel, Nature (London) **337**, 447 (1989).
[5] H. T. Nguyen, A. Bouchta, L. Navailles, P. Barois, N. Isaert, R. J. Twieg, A. Maaroufi, and C. Destrade, J. Phys. II **2**, 1889 (1992).
[6] W. Kuczynski and H. Stegemeyer, Mol. Cryst. Liq. Cryst. Sci. Technol., Sect. A **260**, 377 (1995).
[7] P. A. Pramod, R. Pratibha, and N. V. Madhusudana, Curr. Sci. **73**, 761 (1997).
[8] A. C. Ribeiro, P. Barois, Y. Galerne, L. Oswald, and D. Guillon, Eur. Phys. J. B **11**, 121 (1999).
[9] G. Srajer, R. Pindak, M. A. Waugh, J. W. Goodby, and J. S. Patel, Phys. Rev. Lett. **64**, 1545 (1990).
[10] L. Navailles, P. Barois, and H. T. Nguyen, Phys. Rev. Lett. **71**, 545 (1993).
[11] L. Navailles, H. T. Nguyen, P. Barois, N. Isaert, and P. Delord, Liq. Cryst. **20**, 653 (1996).
[12] L. Navailles, R. Pindak, P. Barois, and H. T. Nguyen, Phys. Rev. Lett. **74**, 5224 (1995).
[13] M. Petit, P. Barois, and H. T. Nguyen, Europhys. Lett. **36**, 185 (1996).
[14] L. Navailles, B. Pansu, L. Gorre-Talini, and H. T. Nguyen, Phys. Rev. Lett. **81**, 4168 (1998).
[15] J. W. Goodby, A. Petrenko, M. Hird, R. A. Lewis, J. Meier, and J. C. Jones, Chem. Commun. (Cambridge) No. 13, 1149 (2000).
[16] A. S. Petrenko, M. Hird, R. A. Lewis, J. G. Meier, J. C. Jones, and J. W. Goodby, J. Phys.: Condens. Matter **12**, 8577 (2000).
[17] A. M. Levelut, E. Hallouin, D. Bennemann, G. Heppke, and D. Loetzsch, J. Phys. II **7**, 981 (1997).
[18] A. M. Levelut, D. Bennemann, G. Heppke, and D. Lotzsch, Mol. Cryst. Liq. Cryst. Sci. Technol., Sect. A **299**, 433 (1997).
[19] J. G. Meier, P. Rudquist, A. S. Petrenko, J. W. Goodby, and S. T. Lagerwall, Liq. Cryst. **29**, 179 (2002).
[20] C. Bahr and G. Heppke, Liq. Cryst. **2**, 825 (1987).
[21] F. Giesselmann and P. Zugenmaier, Phys. Rev. E **55**, 5613 (1997).
[22] B. Jin, Z. Ling, Y. Takanishi, K. Ishikawa, H. Takezoe, A. Fukuda, M. A. Kakimoto, and T. Kitazume, Phys. Rev. E **53**, R4295 (1996).
[23] S. T. Lagerwall, *Ferroelectric and Antiferroelectric Liquid Crystals* (Wiley-VCH, Weinheim, 1999).
[24] I. Dahl and S. T. Lagerwall, Ferroelectrics **58**, 215 (1984).
[25] S. T. Lagerwall and I. Dahl, Mol. Cryst. Liq. Cryst. **114**, 151 (1984).
[26] T. Carlsson, B. Zeks, A. Levstik, and R. Blinc, Mol. Cryst. Liq. Cryst. **163**, 223 (1988).
[27] T. Carlsson, I. W. Stewart, and F. M. Leslie, Liq. Cryst. **9**, 661 (1991).
[28] T. Carlsson, F. M. Leslie, and N. A. Clark, Phys. Rev. E **51**, 4509 (1995).
[29] T. Carlsson and I. Dahl, Mol. Cryst. Liq. Cryst. **95**, 57 (1983).
[30] C. C. Huang and S. Dumrongrattana, Phys. Rev. A **34**, 5020 (1986).
[31] M. Petit, M. Nobili, and P. Barois, Eur. Phys. J. B **6**, 341 (1998).